



A multiplexed immuno-sensor for on-line and automated monitoring of tissue culture protein biomarkers

Zeinab Ramshani^a, Fei Fan^b, Alicia Wei^b, Miguel Romanello-Giroud-Joaquim^b, Chang-Hyun Gil^c, Matt George^d, Mervin C. Yoder^d, Donny Hanjaya-Putra^{a,b}, Satyajyoti Senapati^{a,*}, Hsueh-Chia Chang^{a,b,**}

^a Department of Chemical and Biomolecular Engineering, University of Notre Dame, IN 46556, USA

^b Department of Aerospace and Mechanical Engineering, Bioengineering Graduate Program, University of Notre Dame, IN 46556, USA

^c Department of Surgery, Indiana University School of Medicine, Indianapolis, IN 46202, USA

^d Vascugen Inc., 5602 Research Park Blvd, Ste 213, Madison, WI 53719, USA

ARTICLE INFO

Keywords:

Hydrodynamic shear
Multiplexed protein sensor
Nanomembrane
Silica nanoparticles
Tissue engineering

ABSTRACT

Frequent on-line and automated monitoring of multiple protein biomarkers level secreted in the culture media during tissue growth is essential for the successful development of Tissue Engineering and Regenerative Medicine (TERM) products. Here, we present a low-cost, rapid, reliable, and integrable anion-exchange membrane-(AEM) based multiplexed sensing platform for this application. Unlike the gold-standard manual ELISA test, incubation/wash steps are optimized for each target and precisely metered in microfluidic chips to enhance selectivity. Unlike optical detection and unreliable visual detection for the ELISA test, which require standardization for every usage, the AEM ion current signal also offers robustness, endowed by the pH and ionic strength control capability of the ion-selective membrane, such that a universal standard curve can be used to calibrate all runs. The electrical signal is enhanced by highly charged silica nanoparticle reporters, which also act as hydrodynamic shear amplifiers to enhance selectivity during wash. This AEM-based sensing platform is tested with vascular protein biomarkers, Endothelin-1 (ET-1), Angiogenin (ANG) and Placental Growth Factor (PIGF). The limit of detection and three-decade dynamic range are comparable to ELISA assay but with a significantly reduced assay time of 1 h vs 7 h, due to the elimination of calibration and blocking steps. Optimized protocol for each target renders the detection highly reliable with more than 98% confidence. The multiplexed detection capability of the platform is also demonstrated by simultaneous detection of ET-1, ANG and PIGF in 40 µl of the vascular endothelial cell culture supernatants using three-membrane AEM sensor and the performance is validated against ELISA.

1. Introduction

With the increase prevalence of diabetes and obesity among older adults, the cardiovascular diseases remain a major cause of death worldwide [1]. Many cardiovascular events, such as stroke and coronary heart disease, as well as ischemia and peripheral artery disease, strongly correlate with loss of blood supply, leading to loss of cell function, organ failure, and eventually death [2,3]. Consequently, vascular regeneration using stem and progenitor cells to promote the growth of new blood vessels and restore normal vascular function has been proposed as a promising approach for the treatment of cardiovascular diseases [4–6].

In particular, endothelial colony-forming cells (ECFC) express the characteristics of putative endothelial progenitor cells (EPC) and exhibit tremendous therapeutic potential [7,8]. In addition, ECFC can generate vascular networks to support the maturation of Tissue Engineering and Regenerative Medicine (TERM) products and their successful transplantation *in vivo* [9,10]. TERM products rely on the ability to grow human stem cells in biomaterial scaffolds and expand them in bioreactors with the precise mechanical and chemical cues that recapitulate the *in vivo* microenvironment [11–13]. During this complex process, several regulatory factors interact at multiple levels that facilitate tissue development and remodeling [14,15]. We have previously reported that

* Corresponding author.

** Corresponding author. Department of Chemical and Biomolecular Engineering, University of Notre Dame, IN 46556, USA.

E-mail addresses: ssenapat@nd.edu (S. Senapati), hchang@nd.edu (H.-C. Chang).

ECFCs secrete angiogenic factors, such as Angiogenin (ANG), Endothelin-1 (ET-1), and Placental Growth Factor (PIGF) to facilitate vessel morphogenesis and maturation [16,17]. Therefore, monitoring of such growth factors would allow feedback control of TERM maturation by growth factor/nutrient injection or rapid discarding of failed cultures. With the large number of bioreactors in a tissue foundry, automated and on-line monitoring the level of multiple proteins in individual bioreactors can hence allow massive and efficient production of TERM tissues.

Currently, bioreactors can monitor pH, oxygen, and carbon dioxide levels, but there is no commercial automated technology that can monitor protein biomarkers on-line. The most advanced optical protein detection platforms based on luminescence or fluorescence, like the commercially available Luminex® and Ella™, can quantify multiple targets in a single test [18]. However, their optical instrument is expensive and bulky, thus not suitable for on-line monitoring of individual bioreactor [18]. They also require extensive sample prep, which is difficult to automate. The current gold standard for tissue cultures is still the enzyme linked immuno-sorbent assay (ELISA) test [19–21] and other conventional manual methods such as immunostaining, Western blot and colorimetric assay [22–24] for protein concentration measurements show excellent sensitivity and selectivity. However, they are too slow and too personnel-intensive for on-line monitoring. Their long assay time is due to the multiple hours-long incubation, wash and blocking steps, whose durations are controlled by transport and reaction time limitations of the various bioconjugation and dissociation reactions. The protein diffusion time to the bottom of each well of an ELISA plate is typically hours long and the adsorption time scale for blocking agents can be even longer. Most importantly, optical or visual signals of ELISA need to be recalibrated for every user and for every sample due to unavoidable variations in the optical signals because of noise from interfering agents and sensitivity to sample volume and reagent concentration, both of which can vary because of differences in pipetting techniques. This calibration step for every sample immediately eliminates ELISA as a candidate for automated TERM monitoring.

Lateral flow assay (LFA) is a relatively new immunoassay that uses capillary wetting flow to convect the analytes and reporters to the probes, thus reducing the diffusive transport time to minutes. However, the sensitivity of LFA is limited by visual colorimetric detection. The recent advancement in LFAs development included several signal amplification strategies to enhance detection sensitivity [25]. Some of the recent strategies include the use of colloidal gold nanoparticles (GNPs) with silver enhancement technology [26,27] or the use of a combination of GNPs with signal amplified enzymes (such as horseradish peroxidase [28]). However, the assay remains semi quantitative and not very selective as no washing step is involved during assay. A recent comparative study by Bastos et. al. on COVID-19 serological samples show a significant number of false positives with LFA compared to ELISA [29]. Hence such assays require high affinity antibodies. Further, the performance is dependent on sample complexity and viscosity, thus making them unsuitable for automated and long-term TERM monitoring [30].

Electrochemical immunoassays are label-free and suitable for miniaturization and integration. However, charge based electrochemical sensors like FET is sensitive to ionic strength due to Debye layer screening. For the common sample buffer, the Debye layer is only a few nm thick. This results in high sensitivity to sample ionic strength, as Debye screening determines what fraction of the charge on the target molecules is detectable in FET capacitance sensing [31,32]. On the other hand, amperometric electrochemical sensor uses redox reporters and hence requires blocking agent on the electrode surface so to prevent unwanted electron transfer reaction. However, even in the presence of surface assembled monolayers many current carriers and inhibitors in the buffer can still participate in the electrochemical process, making them unstable and is difficult to calibrate [33]. As the blocking agents are electrostatically adsorbed on the sensor surface, it is quite likely that

the blocking agents can detach from the surface during the washing steps. This can produce large noise or error and false positives. A blocking agent can also influence the performance of porous sensors, such as alumina membrane sensor, by blocking their pores and affecting the target blockage current signal [34], while this effect can be minimized by nano meter pore sized membrane. Therefore, electrochemical sensors often suffer from robustness issues and require careful sample prep, which cannot be easily automated, or individual sample calibration like ELISA.

We aimed to address these challenges by utilizing an anion-exchange membrane (AEM) platform for absolute quantification of multiple protein biomarkers in the tissue samples. The AEM sensors do not require any blocking agents (or sample prep). The entire membrane surface is a sensor that measures the ion current through the membrane, thus eliminating non-specific electrode redox reactions that plague electrochemical sensing. The charged and hydrophilic membrane surface also minimizes non-specific adsorption of proteins. AEM sensors are insensitive to buffer ionic strength, sample pH and chemical composition of the biosamples because of a unique ion depletion action described below [35]. They can be integrated into small-volume biochips to significantly reduce the analyte diffusion time. Flow in the microfluidic chip and on-chip concentration technologies can be used to reduce the transport time further [36]. We have achieved assay time as low as 30 min for nucleic acids that typically require several hours to incubate in a static microarray [37]. All the wash and incubation steps can both be automated and precisely metered for the biochip. The washing step, in particular, can be tuned for each target, to further enhance specificity. This selectivity-enhancing protocol is absent in all other sensor assays. It allows the establishment of a universal protocol that can be used for every target.

Importantly, the AEM sensor relies on electrical measurements, rather than optical ones, thus reducing the instrument cost and robustness considerably and yet retaining the same detection sensitivity. Tedious calibration for every new sample and user is avoided. Probes are attached to the membrane surface to capture the molecular targets. When an electric field is applied across an AEM during sensing, ion depletion occurs within one radius of the circular membrane due to its inherent ion-selectivity characteristics [35] to remove all ions and mobile charged molecules within that neighborhood. The ion depletion is responsible for a limiting-current region within certain voltage interval (typically 1–10 V), where the differential resistance is much higher (>10x) than at lower voltages and, in some cases, infinite. At higher voltages, an overlimiting current region develops on the depleted side when an electro convective instability sets in Ref. [35]. The limiting and overlimiting ion currents through the membrane are both sensitively gated by large negatively charged molecules like nucleic acids bound to the AEM [38]. The ion depletion action increases the Debye length on the membrane (to about 100 nm of DI water) and intensifies the field between negatively charged surface molecules and the positively charged AEM membrane [39,40]. These high-intensity surface electric fields significantly reduce both the field and ion flux into the membrane, thus sensitively shifting the limiting and overlimiting currents. We hence use membrane functionalized oligos to capture nucleic acid targets to produce large voltage signals (100 mV–1 V) for nucleic acid detection and quantification in the pM to nM range [41]. These signals are much larger than those in electrochemical sensor and yet, because there is no redox reaction, it is not contaminated by spurious reactions at high voltages and do not require blocking agents. The size of nucleic acid also allows us to shear non-specifically bound molecules with the high shear rate of microfluidic flow in our chips. We find that our universal calibration curve can be used repeatedly [37,39,40].

However, the protein growth factors are too weakly charged and too small to provide gating of the ionic limiting and overlimiting currents through the membrane and allow specificity enhancement with the high shear of microfluidic flow. Instead, a negatively charged silica nanoparticle reporter with functionalized reporter antibody is used in a

sandwich scheme (Fig. 1a). The local fields between these negatively charged nanoparticles and the positively charged membrane produce large reduction in the overlimiting current comparable to nucleic acids. Additionally, the nanoparticle size and hydrophobicity due to detection antibodies also contribute towards suppression of the electroconvective instability. The same hydrodynamic amplification increases the effect of hydrodynamic shear to remove non-specifically bound nanoparticles on the AEM surface to enhance detection selectivity. With our automated wash protocol, the wash step with a wash buffered is optimized and precisely metered. It is hence expected to render the platform more specific than manual washing.

These advantages of robust pH, ionic strength and signal control of the AEM platform and the universal wash protocol with the nanoparticle reporter allow us to develop a calibration-free automated TERM biomarker monitoring system. Other than calibration free, its other advantages include short incubation time not limited by diffusion or blocking agent adsorption, high selectivity due to automated wash/incubation protocol for each target, low-cost equipment (micropump/potentiostat), insensitivity towards contaminants (no sample prep), multiplex feasibility and comparable sensitivity performance to ELISA. Here, we demonstrate the simultaneous detection of three important angiogenic proteins secreted by ECFCs, PIGF, ANG and ET-1, in less than an hour, compared to 7 h for the corresponding ELISA tests, all based on the same target-specific wash protocol and a universal calibration curve. We have selected these three biomarkers as they are critical for the culture of endothelial colony-forming cells (ECFCs) isolated from the cord blood [8,17]. Previously, using a proteomic analysis we have screened ECFC-conditioned medium and identified several soluble proteins, which are abundant in ECFC-conditioned medium [16,42]. In

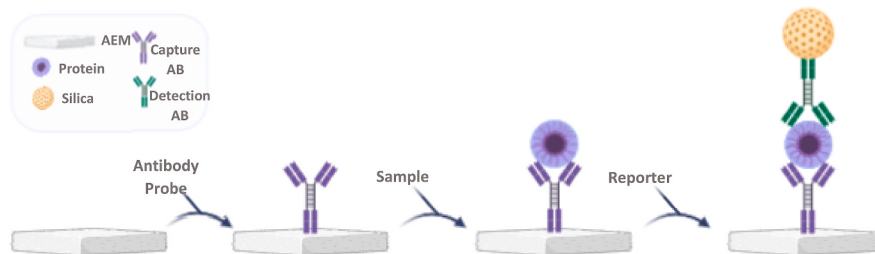
order to minimize any background noise, ET-1, ANG, and PIGF were specifically chosen because they were not present in culture medium while being abundant and important for vascular maturation and functionality. The role of these three biomarkers in maintaining ECFC culture, as well as promoting vascular maturation and functionality are highlighted in Table 1. Although we will only demonstrate its potential with three targets, scaling up to more targets should be straight forward. While we have focused on tissue culture applications, the advantages of this platform also apply to other point-of-care applications, including infectious disease control.

Table 1

Protein biomarkers and maintaining ECFC culture, vascular maturation, and functionality.

Target Protein Biomarker	Capture Antibody (Probe)	Detection Antibody (Reporter)	Protein Antigen (Standard)
Endothelin-1	ab117757 abcam	H00001906-M01 Novus Biologicals	aa 1-212 abcam
Angiogenin	Human Angiogenin Antibody Pair, ab241874 abcam	Human Angiogenin Antibody Pair, ab267683 Abcam	265-AN-050/CF R&D
PIGF	Human Angiogenin Antibody Pair, ab267683 Abcam		264-PGB-010/CF R&D

a



b

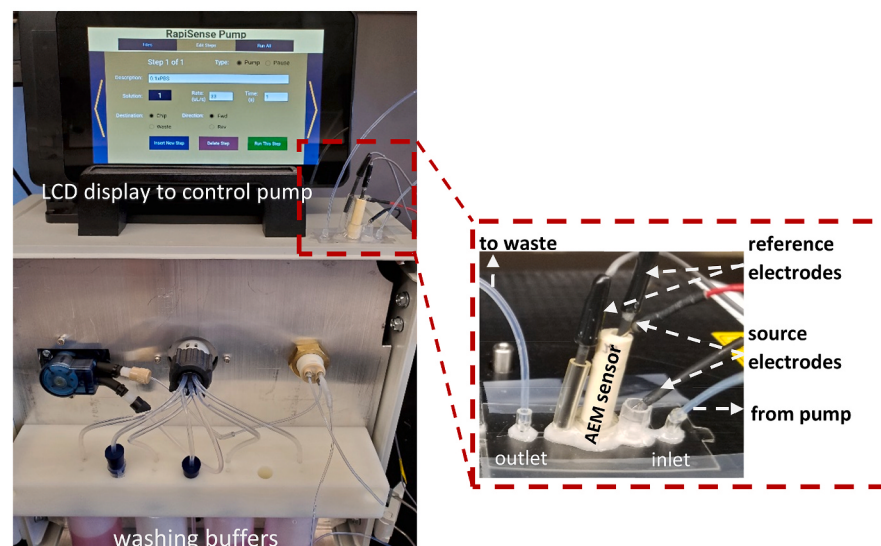


Fig. 1. a) A schematic of AEM-based sandwich assay for protein detection. The AEM functionalized capture antibodies first bind with target proteins present in the sample. Reporter silica particles containing detection antibodies are then allowed to bind with the Ab-Ag adduct that enhance the I-V signal in the overlimiting region of the CVC of AEM. b) A picture of the in-house built fluidic pump, which is used to introduce different assay fluids to biochip. A blow out of the fabricated biochip illustrating the position of four electrodes used for recording of I-V signal.

2. Material and methods

2.1. Fabrication of biochip

The 25 mm × 54 mm ($w \times l$) biochip contains a microfluidic channel that acts as a reservoir for tissue sample and several circular openings to access the microchannel made from three layers of polycarbonate sheet of 0.3 mm thickness using thermal binding (Fig. S1a-c). The details can be found in Supplementary Information under section 1.

The biochip has a sensor chamber to mount a one or multiple membrane sensor module, separate reservoirs to place source and reference electrodes for current-voltage measurement and inlet and outlet for sample and buffer injection.

2.2. Fabrication of nanomembrane sensor

The sensor was made of an anion-exchange membrane (AEM). An AEM is composed of polystyrene-divinylbenzene fine particles with strong basic quaternary ammonium groups supported by polyethylene as a binder and polyamide/polyester textile fiber with a pore size of less than 10 nm (Mega a.s., Czech Republic). The details can be found in Supplementary Information under section 2 “Fabrication of nanomembrane sensor” and Fig. S2. For protein detection, the fabricated AEM sensor was first functionalized with target specific primary antibodies using EDC coupling chemistry as described in previous work [37].

2.3. Preparation of fluorescently labeled carboxylated photoinitiator and protein probes

For efficient and reliable detection of protein biomarkers, an optimized functionalization protocol was developed so that sensors always contain a similar number of protein probes on their surface. As the surface of the membrane is composed of polyethylene materials and does not contain any reactive group, the protein probes were attached in two steps. First, -COOH functional groups were created on the membrane surface by UV irradiation of carboxylated benzophenone. As a result, a free radical generates that undergoes hydrogen abstraction reaction and selectively converts -C-H bond on membrane surface to -COOH. More details on preparing a carboxylation fluorescent mixture, containing the fluorescently labeled ssDNA conjugated 4-Benzoylbenzoic acid in DMSO can be found in Supplementary Information under section 3. “Fabrication and on-chip purification of fluorescently labeled ssDNA conjugated 4-Benzoylbenzoic acid”.

For optimization of the functionalization process, antibody protein probes were fluorescently labeled using Alexa Fluor™ 488 Antibody Labeling Kit. More detailed information can be found in Supplementary Information under section 3. “Fabrication and on-chip purification of fluorescently labeled ssDNA conjugated 4-Benzoylbenzoic acid”. The fluorescently labeled antibody proteins were then linked to the membrane surface by coupling the generated -COOH groups, prepared using the optimized UV treatment carboxylation method, and -NH₂ groups present on the protein molecules using EDC chemistry. The functionalization protocol was optimized by measuring the fluorescence intensity of the attached molecules. More detailed results can be found in Supplementary Information under section 7 “Optimization of primary antibody functionalization protocol on the AEM sensor”.

2.4. Fabrication and on-chip purification of fluorescently labeled ssDNA conjugated 4-benzoylbenzoic acid

In order to purify the fluorescently labeled molecules, a purification chip was constructed. First, a 3 mm thick PMMA block was cut using a micro milling machine (iModela 01). The chip contained a main microfluidic channel (5 mm × 60 mm × 3 mm ($w \times l \times h$)), a cross channel for collection of isolated samples (2 mm × 19 mm × 3 mm ($w \times l \times h$)), a small window to access the cross channel from backside and six

openings for applying voltage across the main channel, loading sample and placing a cation-exchange membrane (CEM) based molecular concentrator (0.9 × 0.3 × 0.3 mm³ ($w \times l \times h$)) as shown in Fig. S3a.

In order to purify the fluorescent mixture and separate the conjugated DNA-benzoylbenzoic acid adduct from the free-floating unconjugated DNA and 4-benzoylbenzoic acid succinimide ester, the main channel was filled with 1 ml of 1% agarose gel (Cat. No. 95057-708, VWR) while the sample loading reservoir and cross channel were kept free of gel. 8 µl of reaction mixture (4-Benzoylbenzoic acid N-succinimidyl ester + FAM labeled ssDNAs) was placed into the sample loading reservoir and 100 V DC voltage (KEITHLEY 2400) at around 2 mA was applied at the end of main channel so that the fast-moving molecules reach the cross channel first and get separated from the fluorescent mixture (Fig. S3b).

Fig. S3c shows the presence of two separate bands in main microfluidic channel, 3 min after applying 100 V DC. The first band is due to the presence of free-floating unconjugated fluorescently labeled DNA in the reaction mixture as its electrophoretic mobility is higher than the conjugated DNA-benzoic acid [35]). After 5 min of applying 100 V DC across the main channel, the free-floating unconjugated labeled DNA (first band in Fig. S3c) crossed the cross channel, so the positive potential probe was switched to the CEM reservoir to concentrate all the conjugated molecules (second band in Fig. S3c) in the cross-channel reservoir as CEM does not allow large co-ions to pass through it due to size constrain. After 7 min, the entire purified fluorescently labeled mixture was concentrated in the cross channel, thus collected from the cross channel was kept at 4 °C and later used for the carboxylation protocol optimization study.

2.5. Optimized functionalization protocol

A droplet of fluorescently labeled 4-Benzoylbenzoic acid purified sample was placed on top of the membrane sensor to cover the AEM sensor surface and soaked for 20 min prior to UV treatment at 365 nm for 80 s with a steady flow of nitrogen gas. The sensor was then vigorously washed with DI water to remove all the unconjugated benzoic acids. This step was repeated 3 times and the sensor was then kept at 0.1 × PBS pH 2 buffer for 4 h before soaking it in 0.1 × PBS at pH 7 and used for the protein probe functionalization. After successful optimization of carboxylation step, the fluorescently labeled protein probes were attached to the sensor surface using EDC coupling chemistry. Briefly, the -COOH modified membrane sensor was first incubated with 0.4 M EDC solution in 1 M MES buffer at pH 5.5 for 40 min. Then a drop of desired protein probe at a concentration of 0.1 mg/ml was then placed on top of the membrane and incubated overnight. The sensor was then washed with 4xPBS to remove any non-specifically adsorbed unconjugated proteins from the sensor surface. The fluorescence intensity was recorded using a CCD camera (Retiga EXi, QImaging) and an inverted fluorescence microscope (Olympus IX71).

2.6. Recording unit and fluidic pump

The fabricated AEM sensor functionalized with the target protein probe was mounted in the biochip so that the sensor surface was in direct contact with samples inside the microchannel. Two platinum electrodes were utilized as source electrodes for current application from 0 µA to final load (two times of limiting current) and two reference electrodes (Ag-AgCl) were used to measure the potential across the membrane sensor at a step rate of 1 µA/s as shown in Fig. 1b. The current voltage characteristics (CVC) of the membrane sensor was established using a Gamry 500 potentiostat (Gamry Instruments, Warminster, PA, USA) connected to a PC for data acquisition and further analysis using Gamry Framework software.

An in-house fluidic pump was designed and built for washing steps using PBS solutions prior to measurements (Fig. 1b). A peristaltic pump which can be run in either direction utilizing a 6in/1 out valve, driven

by a stepper motor was assembled inside an aluminum framework. This fluidic pump was designed to withdraw samples from the reaction chamber, pass it to the biochip and then push reporters and buffers at an optimized flow rate and time. The sterility of the media was protected by the interior six-way valve which prevented any back flow of the fluid from the biochip to the media chamber and no contamination was observed in sterile culture media after the sample withdrawal with this pump. Fluidic controller is accessible via a 7" touchscreen programming interface to define a multi-step washing step including a selection of up to 6 different washing buffers, direction and destination of the fluid in addition to the time and rate of the pumping.

An exemplary I-V curve (CVC) of an AEM sensor is shown on Fig. 2a. The limiting region is a function of the AEM size and considering the manual fabrication of the sensor, different limiting current (I_{lim}) was expected. Hence, the final load of current was decided to be calculated equal to double the limiting current for each AEM individually to keep the voltage shifts comparable between different AEMs. In each experiment the final voltages (V_{final}), before and after target hybridization was compared for individual AEM. Each experiment was performed with a single AEM sensor and no sensor was reused to rule out any detection bias.

3. Results and discussion

3.1. Optimization of primary antibody functionalization protocol on the AEM sensor

Fig. S5 shows the fluorescence images of UV treated membrane surfaces after washing thrice with $4 \times$ PBS buffer to remove any non-specifically adsorbed unconjugated fluorescently labeled –COOH molecules on AEM surface. Fig. S5 clearly indicates the successful carboxylation of the AEM surface, and the mean fluorescent intensity has maximum error of $\pm 1.5\%$ which shows the similarity between the carboxylated sensors is within $\sim 98\%$ of confidence rate.

After successfully optimizing the –COOH printing protocol on the sensor surface, the fluorescently labeled antibody probes were functionalized using EDC coupling chemistry. Fig. S6 clearly shows a very

similar pattern of fluorescent intensities observed after the attachment of fluorescently labeled antibody probes to carboxylated sensors. Similar to previous results with fluorescent –COOH group, we saw the mean fluorescent intensity is almost identical for all sensors with an error of $\pm 2\%$. This indicates that the total number of antibody probes on the sensor surface is almost the same for different sensors. Thus, it demonstrates that the use of this optimized protocol would functionalize a same number of capture antibodies that would allow the target detection reliable and reproducible and the different sensors would detect a target with small error bar.

3.2. Assay protocol

The schematic representation of the biochip and assay steps are shown in Fig. 1a and b As ELISA kit comes with immobilized antibody, we could not use the kit supplied antibodies for our assay. Instead, we screened a list of antibody pairs for PIGF, ANG and ET-1 targets from different vendors with AEM sensor and selected a pair of capture and detection antibodies based on their superior performance. Table 2 shows

Table 2

List of the matching capture antibody, detection antibody and protein antigen.

Protein Biomarker	Size (kDa)	Conc. (pg/mL)	Role in TERM Products	ELISA Kit
Endothelin 1	2.49	30–90	A vasoconstrictor secreted by endothelial cells, which contributes to vascular tone and regulates cell proliferation.	R&D Systems DET100
Angiogenin	14	30–80	A potent stimulator for blood vessel formation.	ThermoFisher EHANG
PIGF	48	800–1600	A homodimer glycoprotein that regulates cell proliferation, migration, and blood vessel formation.	PromoCellPK-EL-66021

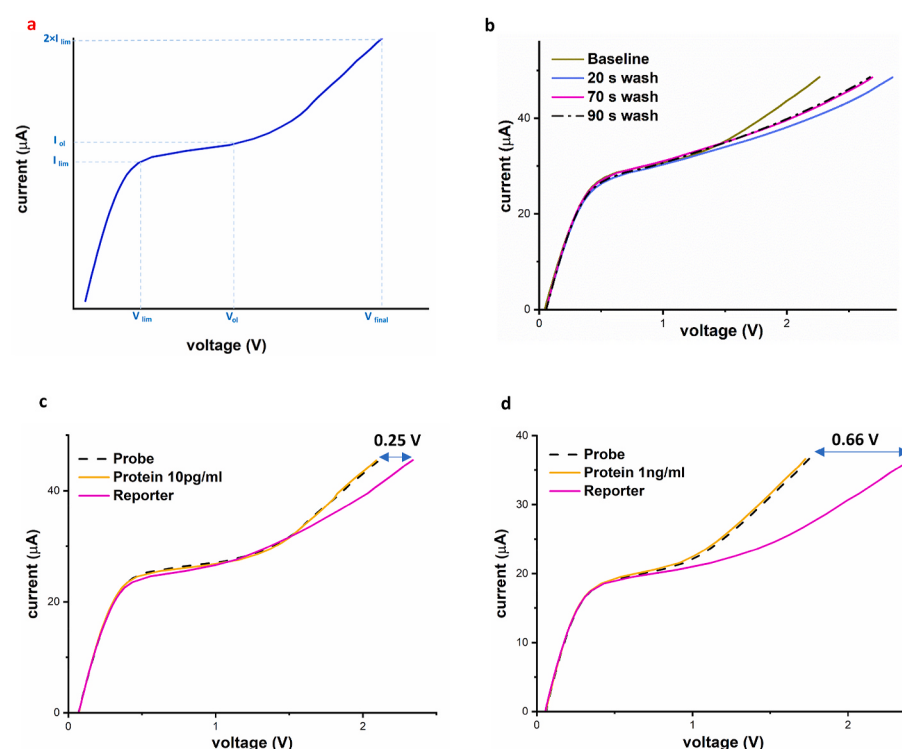


Fig. 2. a) An exemplary I-V curve of an AEM sensor. The transition voltages V_{lim} and V_{el} that de-marcate the under-limiting region, limiting region and over-limiting region are indicated. The CVC terminates at $2 \times I_{lim}$ where the voltage shift is measured, as the curves only change in the over-limiting region. b) Functionalized AEM (green line) was exposed to target protein and reporter and voltage shift was observed (black line). CVC was measured after 20 s (blue), 70 s (magenta) and 90 s (black). Convergence is observed after 70 s of washing. CVC measurements for c) 10 pg/ml of protein ET-1 in 1xPBS and d) 1 ng/ml of protein ET-1 in 1xPBS after convergence utilizing functionalized AEM sensor with ET-1 antibody. (For interpretation of the references to color in this figure legend, the reader is referred to the Web version of this article.)

the selected antigen and antibody pairs for PI GF, ANG and ET-1.

The use of monoclonal antibody as detection antibody on silica reporters along with large hydrodynamic shear drag due to particles would remove any low-affinity non-targets from the sensor surface and hence would enhance the detection selectivity. Additionally, the use of higher reporter concentration can favor rapid binding of monoclonal antibody and can help to reduce the assay time further. However, there is a challenge to find well studied and fully mapped pure capture and detection antibodies for any targets as most of the well validated high binding affinity antibodies are used in ELISA kits.

We hence needed to screen a large number of antibodies that are commercially available and selected the best possible pair that showed promising results with our AEM sensor. Although we used uncharacterized poorly validated antibodies, we were still able to demonstrate a similar detection sensitivity and selectivity, if not better, as ELISA with a comparable error bar.

In a typical experiment, AEM sensor was functionalized with capture antibodies and mounted in the biochip. The CVC measurement was performed with $0.1 \times$ PBS in the microchannel and used as the baseline. $40 \mu\text{l}$ of known concentration of pure antigen sample or tissue sample was then introduced to the microchannel and incubated for 20 min. The sensor was then washed with $2 \times$ PBS and $0.1 \times$ PBS solutions at the flow rate of 2 ml/min to remove the non-specific bounded proteins from AEM surface, $40 \mu\text{l}$ of the detection antibody conjugated silica reporters were injected into the microchannel and incubated for another 20 min. Finally, CVC measurement was conducted after $2 \times$ PBS and $0.1 \times$ PBS solutions at the flow rate of 2 ml/min and the resultant voltage shift was compared with the baseline signal. Fig. 2b shows the convergence of the CVC curve during the 90 s of washing. It is clear that a stable steady-state CVC curve is obtained after 70 s. Non-specifically bound molecules have been sheared off with the metered washing step that can be automated with feedback control of the differential voltage shift in time. This automated wash enabled by electrical signals is a key advantage of the current platform. The concentration of the target protein in sample was then calculated using the relevant calibration formula as discussed in the next section. The total assay time is less than an hour with a limit of detection of 10 pg/ml for ANG and 1 pg/ml for ET-1 targets, shown in calibration curve graphs. The different LOD for ANG and ET-1 targets could be due to the different binding affinity of the selected antibody pairs. Table 3 shows a comparison of our platform with other reported continuous immunoassay-based monitoring system [43–47]. As evident, the LOD of our technology outperforms other reported detection technologies by at least a factor of 2.

Table 3
Comparison of continuous immunoassay-based monitoring systems.

Sensing technology	Target Detected	LOD	Ref
Surface acoustic wave	Carcinoembryonic antigen in exhaled breath condensate	1.25 ng/ml	[43]
Flow Injection Immunoanalysis	Atrazine, a pesticide in drinking water	1 ng/ml	[44]
Immunoaffinity-chromatography method	IgG from the culture of hybridoma cells	5 $\mu\text{g}/\text{ml}$	[45]
Spectrophotometric Immunoassay	Zearalenone, a mycotoxin in food product	0.4 ng/ml	[46]
Electrophoretic immunoassay	Human insulin-like growth factor-I (IGF-I) in serum sample	0.68 ng/ml	[47]
AEM Platform	Endothelin-1, Angiogenin, PI GF targets of Vascular tissue	1 pg/ml	Current Technology

3.3. Universal calibration curve for vascular endothelial cell culture supernatants

The black dashed line in Fig. 2c represents the baseline of the functionalized sensor. We observed no voltage shift after the introduction of the antigen samples. This suggests that Ab-Ag docked adduct is not charged enough and did not bring enough counter ions to induce significant change in the ion conductance of the AEM sensor and produce a shift. This indicates that there is a need for a reporter that can bring significant change in the ion conductance of the sensor upon binding with the ab-ag adduct and produces a large shift in the CVC characteristics in the overlimiting region. We hence selected a 50 nm carboxylated silica particle as a reporter due to its small size and large negative surface charge and attached to a detection antibody. Our selection of silica particles over other negatively charged molecules such as nucleic acid makes the functionalization easy and straight forward as a simple centrifugation step can be used during conjugation of antibodies. Further, the high density of silica particles enhances the detection selectivity as the large shear drag force exerted by the particles during washing can remove the low affinity or non-specifically bounded non-targets [48]. The details of conjugating silica particles and reporter preparations can be found in Supplementary Information under section 4. After incubation with the silica reporters, the CVC measurement showed a shift of $\sim 0.25 \text{ V}$ for $10 \text{ pg}/\text{ml}$ and $\sim 0.66 \text{ V}$ for $1 \text{ ng}/\text{ml}$, thus clearly indicating the successful capture of the targets (Fig. 2c and d).

After successful optimization of the assay protocol, a calibration plot was developed for ET-1 and ANG. As expected, a gradual increase in voltage is observed with the increase in protein concentration. Triplicate study also shows a linear increase in voltage with a small error bar of 0.01 V with a 95% confidence rate. The calibration plots thus developed was used to determine the protein concentration present in vascular endothelial cell culture supernatants.

Fig. 3a indicates the logarithmic relation between the ET-1 protein concentration and measured voltage shift by this formula:

$$\Delta V_v = (175 \times 10^{-5}) + (0.095) \times \ln(C_{\frac{\text{pg}}{\text{ml}}} + 5) \quad (1)$$

Where C is the concentration of ET-1 in pg/ml and ΔV is the recorded voltage shift in volt.

To assess the detection efficacy of this sensing chip, a series of experiments were conducted using vascular endothelial cell culture supernatants. The details of the cell isolation preparations and ELISA assay are explained in detail in Supplementary Information under section 5 and 6, respectively. The triplicate measurements with different AEM sensors showed a comparable ET-1 concentration with ELISA in vascular endothelial cell culture supernatants. AEM sensor indicated the presence of $50.00 \pm 1.60 \text{ pg}/\text{ml}$ ET-1 concentration versus $38.00 \pm 0.26 \text{ pg}/\text{ml}$ as observed with ELISA (Fig. 3b). This study clearly indicates that the performance of our AEM sensor is as good as ELISA with a significantly lower assay time, 1 h as compared to 7 h for ELISA. It is pertinent to mention that although the antibody pair used in the AEM sensor may have a low binding affinity for the target antigen, but still the detection sensitivity at par with ELISA.

Similarly, we tested the selected antibody pair for another vascular protein biomarker, ANG, and developed a calibration plot. As shown in Fig. 3c, the limit of detection of ANG protein was 1 pg/ml and the sensing platform exhibited log-linear behavior over 3 decades of concentration. The Ang protein concentration (C in pg/ml) and voltage shift (ΔV in V) are logarithmically related by:

$$\Delta V_v = 0.25 + 0.1 \times \ln(C_{\frac{\text{pg}}{\text{ml}}} + 0.84) \quad (2)$$

The performance of AEM sensor was benchmarked with ELISA by measuring the concentration of the ANG protein in the vascular endothelial cell culture supernatants sample. Fig. 3d shows the ANG concentration in tissue samples as measured by ELISA. The concentration of

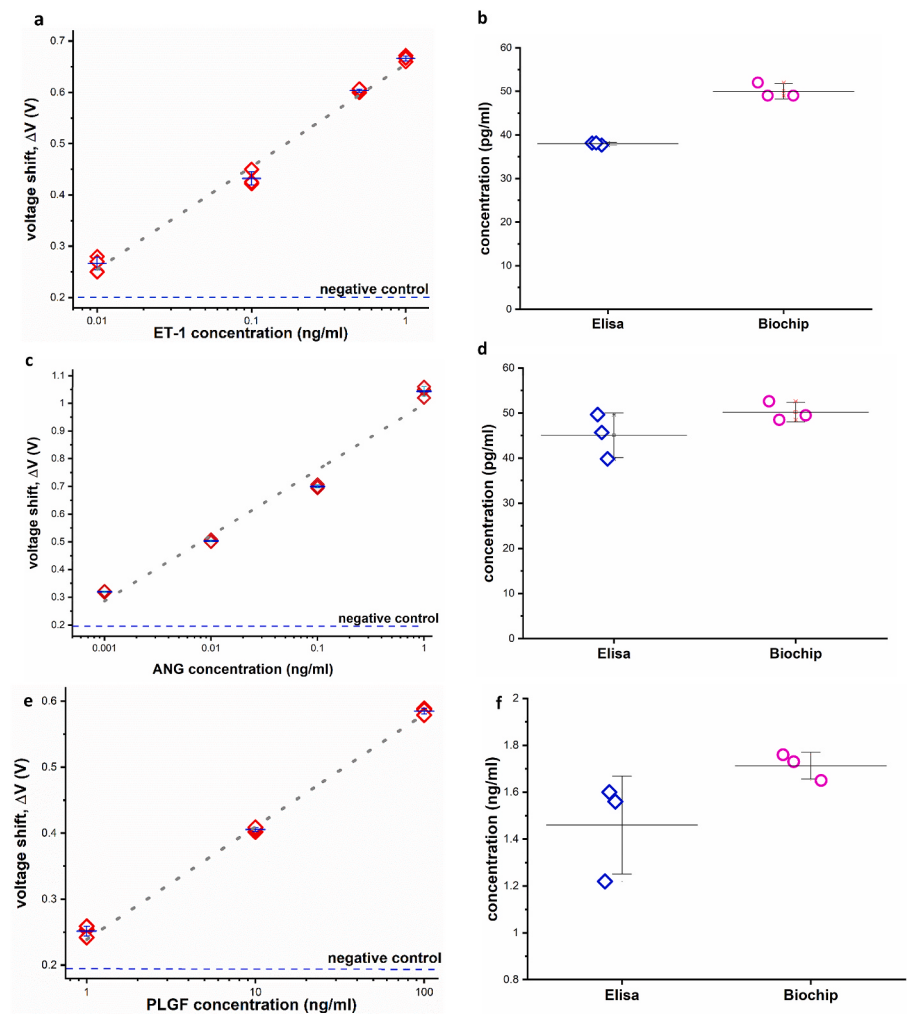


Fig. 3. a) A calibration plot for ET-1 protein produced by AEM platform after measuring voltage shift at different ET-1 protein concentration. Each point indicates the average of three replicates of the same concentration, using three functionalized AEM sensor. b) Implementing the ET-1 calibration plot, the concentration of the ET-1 protein in vascular endothelial cell culture supernatants were measured using AEM platform and benchmarked against ELISA ($n = 3$). c) A calibration plot for ANG protein produced after recording voltage shift at different ANG protein concentration. Each point indicates the average of three replicates of the same concentration using three functionalized AEM sensor. d) Benchmarking AEM platform against ELISA in detecting the concentration of ANG protein in vascular endothelial cell culture supernatants ($n = 3$). e) A calibration plot for PI GF protein using produced voltage shift at different PI GF protein concentration. Each point indicates the average of three replicates of the same concentration using three functionalized AEM sensor. f) Benchmarking AEM platform against ELISA in detecting the concentration of PI GF protein in vascular endothelial cell culture supernatants ($n = 3$).

ANG was found to be 45.0 ± 4.5 pg/ml, which is comparable to the concentration of 50.0 ± 1.9 pg/ml obtained using AEM sensor.

In the last attempt, the calibration plot for the third vascular protein biomarker, PI GF was established. Fig. 3e, indicates the limit of detection 1 ng/ml for PI GF protein. According to the calibration plot, the PI GF protein concentration (C in pg/ml) and voltage shift (ΔV in V) are logarithmically related by:

$$\Delta V_v = 0.22 + 0.08 \times \ln\left(\frac{C_{\text{ng}}}{\text{ml}} + 0.5\right) \quad (3)$$

The performance of AEM sensor was benchmarked with ELISA by measuring the concentration of the PI GF protein in the vascular endothelial cell culture supernatants sample. Fig. 3f shows the PI GF concentration in vascular endothelial cell culture supernatants samples as measured by ELISA. The concentration of PI GF was found to be 1.46 ± 0.17 ng/ml, which is comparable to the concentration of 1.71 ± 0.04 ng/ml obtained using AEM sensor.

While the benchmarking results are comparable with ELISA, the slight difference in biomarkers concentration can be due to different binding affinity of the used antibody pairs for these two biomarkers. The biochip data show much smaller standard deviation, which should be a result of our standardized wash protocol. Importantly, quantification of the biochip data for all the samples in Fig. 3b, d and f are based on the universal calibration curve of Fig. 3a, c and e, whereas the ELISA tests require a separate calibration for each data point.

3.4. Negative control experiments and wash protocol optimization

To ensure that the I-V shift observed in Figs. 2 and 3 are in fact due to the presence of ET-1 and ANG targets in vascular endothelial cell culture supernatants, a series of negative control experiments were conducted. First, the effect of silica reporters on the detection antibody was tested by exposing the reporter to a sensor functionalized with capture antibodies for 30 min. Fig. 4a, shows a small shift of 0.18 V after washing with $2 \times$ PBS at a flow rate of 2 ml/min. This suggests that $2 \times$ PBS wash buffer is not sufficiently strong enough to detach all non-specifically adsorbed silica reporters on the AEM surface. Although we can remove the silica reporter completely and bring the I-V to baseline with higher flow rate or more than $2 \times$ PBS conducting wash buffer but we observed that both approaches can detach Ab-Ag-Ab adduct from the AEM surface and we do not see any I-V shift. We hence considered this small shift as a background noise of the sensor and any shift more than 0.2 V are considered due to the presence of target.

As a second strategy, the sensor was exposed to a mixture of proteins and miRNAs spiked-in media sample to check whether our sensor is selective enough as tissue bioreactor samples would contain several free-floating non-target proteins and nucleic acids. Hence, the media sample was spiked with 1 ng/ml of non-target protein (PI GF) and 1 nM of non-target miRNA (miR-208) and exposed to ET-1 captured antibody functionalized AEM sensor. The related reporter was then incubated inside the microchannel for 30 min. CVC measurements were then performed after washing with $2 \times$ PBS at 2 ml/min flow rate. A voltage shift of 0.19 V (Fig. 4b) was recorded which is very similar to the 0.18 V shift that

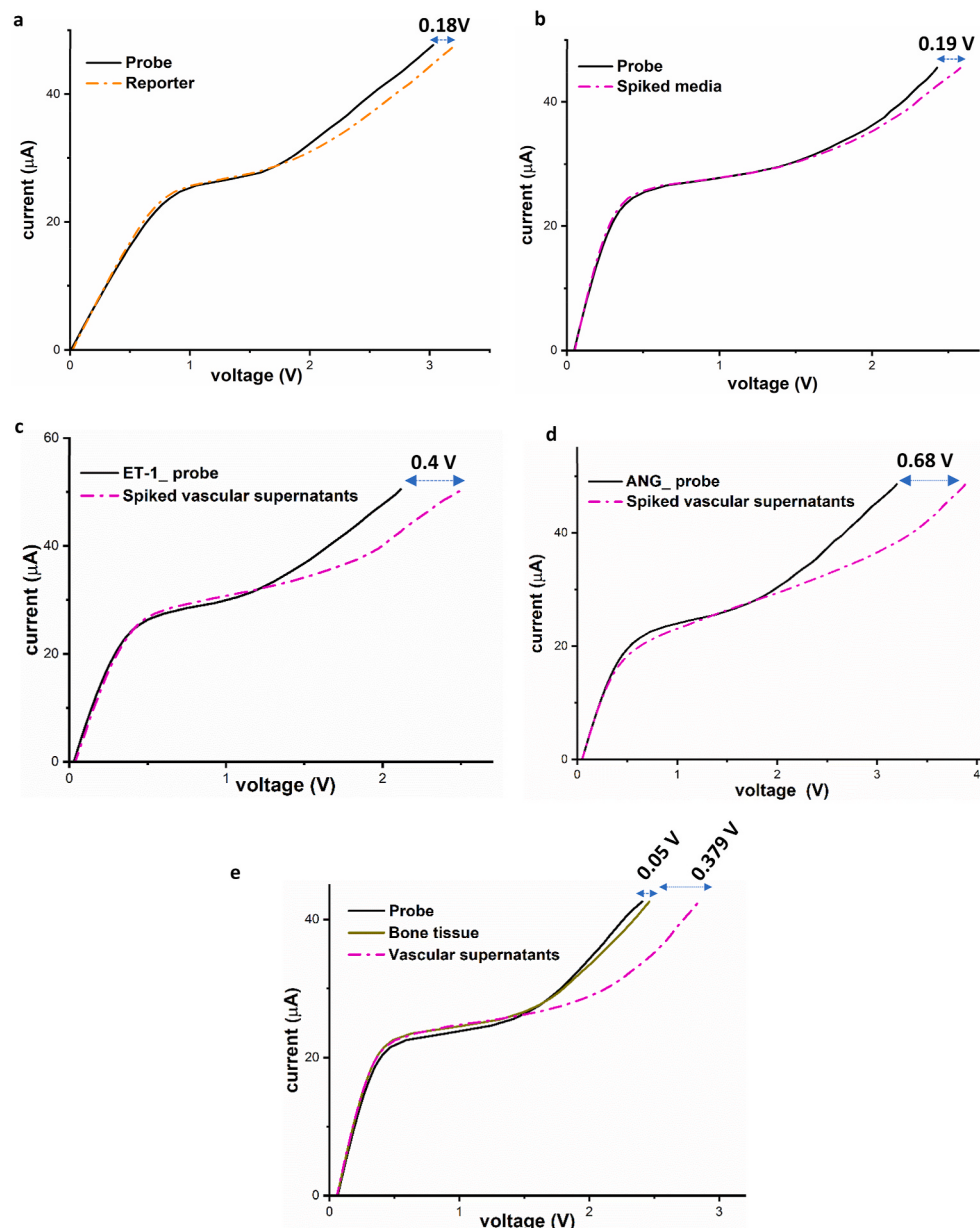


Fig. 4. A series of negative control experiments were conducted to validate the AEM platform. a) The ANG reporter was incubated with AEM sensor functionalized with angiogenin probe and a 0.18v voltage shift was recorded. b) Tissue media sample spiked with 1 nM of miRNA (mir-208) and 1 ng/ml of non-target protein PLGF was incubated with a sensor functionalized with ET-1 antibody probe. A voltage shift of 0.19v was measured after incubating with ET-1 reporter. CVC measurements of functionalized AEMs exposed to vascular endothelial cell culture supernatants spiked with non-target protein c) 1 ng/ml of PI GF protein d) 1 ng/ml of Osteonectin protein. Voltage shifts are within the 95% confidence range of non-spiked vascular endothelial cell culture supernatants sample obtained in Fig. 3b-d e) Voltage shift for bone tissue sample is negligible for the ET-1 probe functionalized AEM while the vascular endothelial cell culture supernatants sample shows 0.379 V voltage shift using the same AEM sensor, consistent with our previous results obtained in Fig. 3b.

observed when we only used silica reporters in Fig. 4a.

As a third strategy, we also tested whether the selected antibody pairs are selective and do not cross react with other proteins. In other word, the selected antibody pairs for each target protein does not bind with any other non-target proteins. In order the check it, we spiked-in 1 ng/ml of PI GF to vascular endothelial cell culture supernatants sample and exposed to AEM functionalized with ET-1 probe. Similarly, we spiked-in 1 ng/ml of non-target protein (Osteonectin, SPARC) and exposed to AEM functionalized with ANG probe and related reporters prior to the CVC measurements. As shown in Fig. 4c-d, a shift of 0.401 V and 0.687 V were observed for ET-1 and ANG functionalized AEMs respectively, which is within the 95% confidence range of our previous results in Fig. 3b and d. Additionally, it detects the amount of ANG and ET-1 targets that are expected to be present in conditioned medium from vascular tissue samples as observed previously in Fig. 3.

Finally, the capability of a functionalized sensor in distinguishing between the target protein in a complex sample after exposing to non-target protein was verified. ET-1 probe was printed on the AEM sensor and exposed to bone tissue samples. Our ELISA study shows that bone

tissue samples does not contain ET-1 target and hence this sample is a realistic negative control sample since it will contain all relevant biomolecules released by bone tissue during its proliferation. As seen in Fig. 4e, no significant voltage shift ($\Delta V = 0.05$ V) was observed, thus suggesting high detection selectivity of the sensor. Just to make sure that the sensor indeed contains the ET-1 probe, we then introduced vascular endothelial cell culture supernatants sample (used in Fig. 3) and related reporter. As expected, a voltage shift of 0.379 V was recorded (Fig. 4e), which is within 95% confidence range of our previous study (Fig. 3b). This clearly demonstrates that AEM sensor highly sensitive and selective towards the target despite the presence of non-target proteins and other biomolecules in tissue samples.

3.5. Simultaneous detection of ANG and ET-1 targets in vascular endothelial cell culture supernatants

After successfully validating the performance of individual target with AEM sensor, a two-membrane sensor was fabricated for simultaneous detection of both ANG and ET-1 targets from vascular tissue

samples in a single test. In brief, two-membrane sensor was fabricated by placing two pieces of membranes on a single disk separated by two isolated chambers so that each sensor functions independent of each other and avoids any cross talk in I-V measurement (Fig. 5a and b). First, ANG and ET-1 probes were attached on each carboxylized membrane sensor. The functionalized two-membrane sensor was then placed in the biochip and exposed to vascular tissue samples for 30 min. We then exposed the sensor to ET-1 silica reporters and measured I-V signal after washing with the optimized protocol developed with single target. A shift of 0.379 V was observed for ET-1 sensor while no shift was observed for ANG sensor (Fig. 5c). The sensor was then exposed to ANG reporter and I-V signal was recorded. A shift of 0.66 V was observed for ANG sensor while no additional shift was observed for ET-1 sensor (Fig. 5c). This clearly demonstrates the successful detection of both targets present in the tissue sample. Additionally, the extent of voltage shift observed for both the targets were very similar to the shift that observed for individual targets (Fig. 3b for ET-1 and Fig. 3d for ANG).

Fig. 5d shows the detection consistency of the measured voltage shifts in two-membrane sensor, where we witnessed less than 2% variations in voltage measurements for both AEMs. The triplicate experiment results of the two-membrane sensing system were then benchmarked against ELISA as shown in figure (Fig. 5e). The first two-column in Fig. 5e, indicating the biochip results, are produced using 40 μ l of sample in 1 h while the second two columns representing the ELISA results are obtained using two separate ELISA kits, each requires around 8 h, since there is no commercially available ELISA kit which is capable of simultaneous detection of both ET-1 and ANG. This clearly indicates the multiplexed capability of our AEM sensor.

3.6. Demonstration of performance of three-membrane sensor

To further check the capability of our AEM sensor in identifying three or more targets simultaneously in a single test, a 3-membrane sensor was fabricated. Due to difficulty in identifying the antibody pairs for third vascular target, a single target was picked to demonstrate the detection capability of three-membrane sensor. Hence the same probe was attached on all three membrane sensors and exposed to vascular endothelial cell culture supernatants to check whether all three sensors show the similar I-V shift. This experiment was necessary to prove whether the optimized functionalization protocol is reliable for multi target detection and whether we can detect the same number of targets with a similar error bar. Similar to two-membrane sensor, a well separated three-membrane sensor isolated by three separate chambers was fabricated as shown in Fig. 6 a. ET-1 probes were then functionalized to each sensor and exposed to vascular endothelial cell culture supernatants in biochip (Fig. 6b). Fig. 6c exhibits the CVC measurements of the three-membrane sensor. A similar voltage shifts were observed in all three sensors. The shift is comparable to the result obtained with single sensor (Fig. 3) with less than 1% error and within the 95% confidence. The different under-limiting and limiting region of CVC characteristics in each sensor is due to heterogeneity of the membrane and that could have different conductance of the sensor membrane. However, despite this, the shift in voltage in all three sensors are identical. This clearly suggests that the accuracy of detection with AEM sensor is mostly dependent on the number of probes printed on the sensor surface and less on surface characteristics. The fact that the results of the study showing less than 1% error between different sensors further confirms the reliability of the

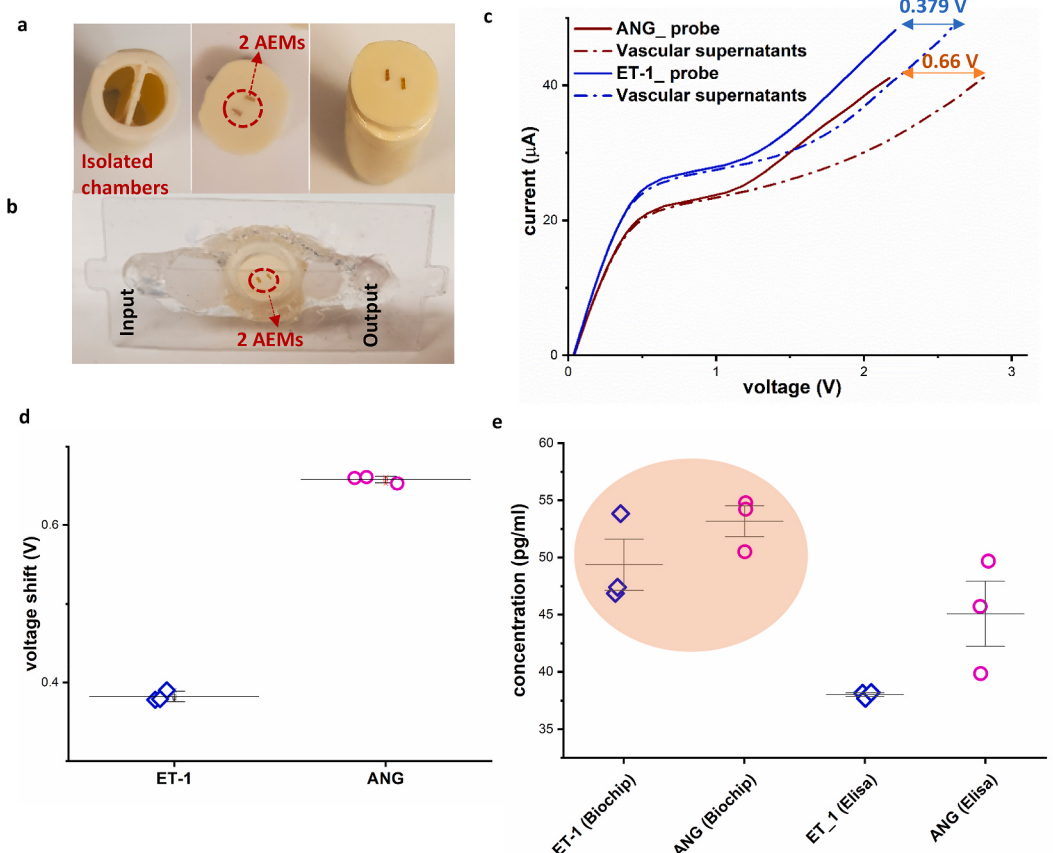


Fig. 5. Simultaneous detection of two protein biomarkers, ET-1 and ANG, in vascular endothelial cell culture supernatants using two-membrane sensor a) Fabrication of the sensor with two separated AEMs and chambers b) Mounting the functionalized two-membrane sensor in biochip. c) CVC measurements of the fabricated two-membrane sensor functionalized with ET-1 and ANG probes after exposing the sensor with vascular endothelial cell culture supernatants. d) Average recorded voltage shifts for both AEMs with less than 2% variations ($n = 3$). e) Simultaneous detection of ET-1 and ANG in vascular endothelial cell culture supernatants using 40 μ l of sample in 1 h benchmarked against ELISA results using two ELISA kits.

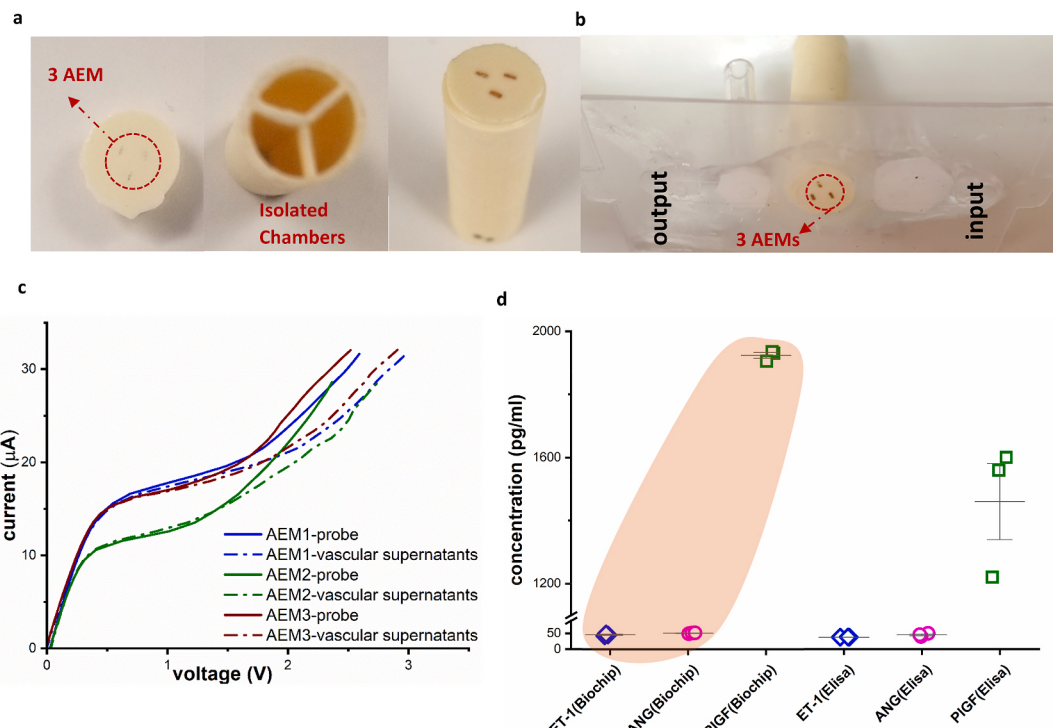


Fig. 6. Three-membrane sensor a) Fabrication of the sensor with three separated AEMs and chambers b) Mounting the functionalized three-membrane sensor in biochip. c) CVC measurements for vascular endothelial cell culture supernatants using all three AEMs of a three-membrane sensor functionalized with ET-1 probe. The shift is comparable to the result obtained with single sensor with less than 1% error and within the 95% confidence. d) Simultaneous detection of ET-1, ANG and PIGF in vascular endothelial cell culture supernatants using 40 μ l of sample in 1 h benchmarked against ELISA results using three ELISA kits.

multiplex sensor. Hence, the integration of the platform with a bioreactor can be used for routine monitoring of multiple targets in vascular tissue samples. To assess the capability of our biochip protein assay towards multiplex detection, three membrane sensors were functionalized using three vascular protein biomarker, ET-1, ANG and PIGF, each printed on an AEM surface. Same washing protocol, sample volume and incubation time was followed as was explained earlier for single membrane protein detection assay. The first three-column in Fig. 6d, indicating the biochip results, are produced using 40 μ l of vascular endothelial cell culture supernatants sample in 1 h while the second two columns representing the ELISA results are obtained using three ELISA kits, to measure the concentration of three protein biomarkers individually, each requires around 8 h, since there is no commercially available ELISA kit which is capable of simultaneous detection of ET-1, ANG and PIGF.

4. Conclusions

We have successfully developed a rapid, low-cost, sensitive, and selective multiplexed sensing platform suitable for automated online monitoring of multiple protein targets in vascular endothelial cell culture supernatants from a single test. Its amenability to on-line automation mainly lies in its target-specific wash protocol and its intrinsic robustness that eliminates individual sample calibration, which result in significant reduction in assay time and processing steps. To validate this technique, a culture of human ECFCs was chosen due to its relevance for various tissue engineering applications, as well as its widespread adoption into various TERM products [2,17]. A sandwich assay strategy is used where detection antibodies conjugated with silica nanoparticles act as a reporter to gate the ionic current through a membrane sensor and also as a hydrodynamic shear amplifier to remove non-specifically bound reporters with an automated and precisely metered wash step. The limit of detection of the sensor is comparable to that of ELISA with

significantly less assay time and sample volume. It can detect as low as pg/ml in 1 h in 40 μ l of tissue samples. Further, the use of optimized protocol to functionalize similar number of capture antibodies on the sensor surface makes the sensing highly reliable and reproducible with a small detection error bar within 95% confidence limit. Further, its simple peripheral instrumentation makes the integration with a bioreactor straight forward and can be used for reliable and efficient detection of multiple targets in tissue samples for routine monitoring of the potential biomarkers released during the maturation of various TERM products. We previously demonstrated that the AEM sensor can be used to detect four dengue serotypes simultaneously from a single test [40] and hence it can be easily scaled up to identify more than four targets by placing multiple four-membrane sensor modules in a series in a single microfluidic channel or one sensor module in four channels that emanate from the sample reservoir [49].

Author contribution statement

H.-C. C., D. H.-P., and S. S. led and organized the project. Z. R. and S. S. designed, engineered, fabricated, tested, and optimized the platform. Z. R. conducted all the experiments with biochip and developed figures. F. F. and A. W. performed cell culture isolation and ELISA assays. M. R. G.-J. contributed to sensor fabrication and helping in running the experiments. C.H.G. has performed the ECFC isolation and culture and prepared the supernatants. M.G and M.C.Y contributed to identifying the vascular protein targets and providing the vascular tissue samples. H.-C. C., D. H.-P., S. S. and Z. R. all contributed to writing the manuscript.

Declaration of competing interest

The authors declare that they have no known competing financial interests or personal relationships that could have appeared to influence the work reported in this paper.

Acknowledgements

The authors would like to thank Dr. Olivia Beane and Dr. Sarindr Bhumiratana of EpiBone Inc. NY 11226 for providing the bone tissue samples for control study. "Research was sponsored by the Office of the Secretary of Defense and was accomplished under Agreement Number W911NF-17-3-003. The views and conclusions contained in this document are those of the authors and should not be interpreted as representing the official policies, either expressed or implied, of the Office of the Secretary of Defense or the U.S. Government. The U.S. Government is authorized to reproduce and distribute reprints for Government purposes notwithstanding any copyright notation herein."

Appendix A. Supplementary data

Supplementary data to this article can be found online at <https://doi.org/10.1016/j.talanta.2020.122021>.

References

- [1] E.J. Benjamin, P. Muntner, A. Alonso, M.S. Bittencourt, C.W. Callaway, A. P. Carson, A.M. Chamberlain, A.R. Chang, S. Cheng, S.R. Das, F.N. Delling, L. Djousse, M.S.V. Elkind, J.F. Ferguson, M. Forname, L.C. Jordan, S.S. Khan, B. M. Kissela, K.L. Knutson, T.W. Kwan, D.T. Lackland, T.T. Lewis, J.H. Lichtman, C. T. Longenecker, M.S. Loop, P.L. Lutsey, S.S. Martin, K. Matsushita, A.E. Moran, M. E. Mussolino, M. O'Flaherty, A. Pandey, A.M. Perak, W.D. Rosamond, G.A. Roth, U. K.A. Sampson, G.M. Satou, E.B. Schroeder, S.H. Shah, N.L. Spartano, A. Stokes, D. L. Tirschwell, C.W. Tsao, M.P. Turakhia, L.B. VanWagner, J.T. Wilkins, S.S. Wong, S.S. Virani, Heart disease and stroke statistics-2019 update: a report from the American heart association, *Circulation* (2019), <https://doi.org/10.1161/CIR.0000000000000659>.
- [2] K. Banno, M.C. Yoder, Tissue regeneration using endothelial colony-forming cells: promising cells for vascular repair, *Pediatr. Res.* 83 (2018) 283–290, <https://doi.org/10.1038/pr.2017.231>.
- [3] X. Yao, F. Ye, X. Qingbo, Vascular regeneration by stem/progenitor cells, *Arterioscler. Thromb. Vasc. Biol.* 36 (2016) e33–e40, <https://doi.org/10.1161/ATVBAHA.116.307303>.
- [4] S. Kusuma, Y.-I. Shen, D. Hanjaya-Putra, P. Mali, L. Cheng, S. Gerecht, Self-organized vascular networks from human pluripotent stem cells in a synthetic matrix, *Proc. Natl. Acad. Sci.* 110 (2013) 12601–12606, <https://doi.org/10.1073/pnas.1306562110>.
- [5] N. Prasain, M.R. Lee, S. Vemula, J.L. Meador, M. Yoshimoto, M.J. Ferkowicz, A. Fett, M. Gupta, B.M. Rapp, M.R. Saadatzadeh, others, Differentiation of human pluripotent stem cells to cells similar to cord-blood endothelial colony-forming cells, *Nat. Biotechnol.* 32 (2014) 1151.
- [6] E.A. Silva, E.-S. Kim, H.J. Kong, D.J. Mooney, Material-based deployment enhances efficacy of endothelial progenitor cells, *Proc. Natl. Acad. Sci.* 105 (2008) 14347, <https://doi.org/10.1073/pnas.0803873105>. LP – 14352.
- [7] K.K. Hirschi, D.A. Ingram, M.C. Yoder, Assessing identity, phenotype, and fate of endothelial progenitor cells, *Arterioscler. Thromb. Vasc. Biol.* 28 (2008) 1584. LP – 1595.
- [8] D.A. Ingram, L.E. Mead, H. Tanaka, V. Meade, A. Fenoglio, K. Mortell, K. Pollok, M. J. Ferkowicz, D. Gilley, M.C. Yoder, Identification of a novel hierarchy of endothelial progenitor cells using human peripheral and umbilical cord blood, *Blood* 104 (2004) 2752. LP – 2760.
- [9] Y.-C. Chen, R.-Z. Lin, H. Qi, Y. Yang, H. Bae, J.M. Melero-Martin, A. Khademhosseini, Functional human vascular network generated in photocrosslinkable gelatin methacrylate hydrogels, *Adv. Funct. Mater.* 22 (2012) 2027–2039, <https://doi.org/10.1002/adfm.201101662>.
- [10] D. Hanjaya-Putra, Y.-I. Shen, A. Wilson, K. Fox-Talbot, S. Khetan, J.A. Burdick, C. Steenbergen, S. Gerecht, Integration and regression of implanted engineered human vascular networks during deep wound healing, *Stem Cells Transl. Med.* 2 (2013) 297–306, <https://doi.org/10.5966/sctm.2012-0111>.
- [11] B.M. Frey, S.M. Zeisberger, S.P. Hoerstrup, Tissue engineering and regenerative medicine-new initiatives for individual treatment offers, *Transfus. Med. Hemotherapy* (2016), <https://doi.org/10.1159/000450716>.
- [12] F. Han, J. Wang, L. Ding, Y. Hu, W. Li, Z. Yuan, Q. Guo, C. Zhu, L. Yu, H. Wang, Z. Zhao, L. Jia, J. Li, Y. Yu, W. Zhang, G. Chu, S. Chen, B. Li, Tissue engineering and regenerative medicine: achievements, future, and sustainability in asia, *Front. Bioeng. Biotechnol.* (2020), <https://doi.org/10.3389/fbioe.2020.00083>.
- [13] C.D. Porada, A.J. Atala, G. Almeida-Porada, The hematopoietic system in the context of regenerative medicine, *Methods* (2016), <https://doi.org/10.1016/j.ymeth.2015.08.015>.
- [14] R.M. Nerem, D. Seliktar, Vascular tissue engineering, *Annu. Rev. Biomed. Eng.* (2001), <https://doi.org/10.1146/annurev.bioeng.3.1.225>.
- [15] G. Vunjak-Novakovic, D.T. Scadden, Biomimetic platforms for human stem cell research, *Cell Stem Cell* 8 (2011) 252–261, <https://doi.org/10.1016/j.stem.2011.02.014>.
- [16] R.S. Alphonse, A. Vadivel, M. Fung, W.C. Shelley, P.J. Critser, L. Ionescu, M. O'Reilly, R.K. Ohls, S. McConaghay, F. Eaton, S. Zhong, M. Yoder, B. Thébaud, Existence, functional impairment, and lung repair potential of endothelial colony-forming cells in oxygen-induced arrested alveolar growth, *Circulation* 129 (2014) 2144–2157, <https://doi.org/10.1161/CIRCULATIONAHA.114.009124>.
- [17] D. Hanjaya-Putra, V. Bose, Y.-I. Shen, J. Yee, S. Khetan, K. Fox-Talbot, C. Steenbergen, J.A. Burdick, S. Gerecht, Controlled activation of morphogenesis to generate a functional human microvasculature in a synthetic matrix, *Blood* 118 (2011) 804. LP – 815.
- [18] A. Leligdowicz, A.L. Conroy, M. Hawkes, K. Zhong, G. Lebovic, M.A. Matthay, K. C. Kain, Validation of two multiplex platforms to quantify circulating markers of inflammation and endothelial injury in severe infection, *PLoS One* (2017), <https://doi.org/10.1371/journal.pone.0175130>.
- [19] E. Staples, R.J.M. Ingram, J.C. Atherton, K. Robinson, Optimising the quantification of cytokines present at low concentrations in small human mucosal tissue samples using Luminex assays, *J. Immunol. Methods* (2013), <https://doi.org/10.1016/j.jim.2013.04.009>.
- [20] L. Wu, G. Li, X. Xu, L. Zhu, R. Huang, X. Chen, Application of nano-ELISA in food analysis: recent advances and challenges, *TrAC Trends Anal. Chem.* (Reference Ed.) (2019), <https://doi.org/10.1016/j.trac.2019.02.002>.
- [21] S. Zhang, A. Garcia-D'Angel, J.P. Brennan, Q. Huo, Predicting detection limits of enzyme-linked immunosorbent assay (ELISA) and bioanalytical techniques in general, *Analyst* (2013), <https://doi.org/10.1039/c3an01835k>.
- [22] A.G. Gornall, C.J. Bardawill, M.M. David, Determination of serum proteins by means of the biuret reaction, *J. Biol. Chem.* (1949).
- [23] S. Jung, D.A. Rickert, N.A. Deak, E.D. Aldin, J. Recknor, L.A. Johnson, P. A. Murphy, Comparison of Kjeldahl and dumas methods for determining protein contents of soybean products, *JAOCs*, *J. Am. Oil Chem. Soc.* (2003), <https://doi.org/10.1007/s11746-003-0837-3>.
- [24] J.M. Walker, J.H. Waterborg, The lowry method for protein quantitation, in: *Protein Protocols Handbook*, the, 2003, <https://doi.org/10.1385/1-59259-169-8:7>.
- [25] X. Mao, Y. Ma, A. Zhang, L. Zhang, L. Zeng, G. Liu, Disposable nucleic acid biosensors based on gold nanoparticle probes and lateral flow strip, *Anal. Chem.* (2009), <https://doi.org/10.1021/ac0824653>.
- [26] L. Anfossi, F. Di Nardo, C. Giovannoli, C. Passini, C. Baggiani, Increased sensitivity of lateral flow immunoassay for ochratoxin A through silver enhancement, *Anal. Bioanal. Chem.* (2013), <https://doi.org/10.1007/s00216-013-7428-6>.
- [27] W. Lai, D. Tang, X. Que, J. Zhuang, L. Fu, G. Chen, Enzyme-catalyzed silver deposition on irregular-shaped gold nanoparticles for electrochemical immunoassay of alpha-fetoprotein, *Anal. Chim. Acta* (2012), <https://doi.org/10.1016/j.aca.2012.10.028>.
- [28] C. Parolo, A. de la Escosura-Muñiz, A. Merkoçi, Enhanced lateral flow immunoassay using gold nanoparticles loaded with enzymes, *Biosens. Bioelectron.* (2013), <https://doi.org/10.1016/j.bios.2012.06.049>.
- [29] M. Lisboa Bastos, G. Tavaziva, S.K. Abidi, J.R. Campbell, L.P. Haraoui, J. C. Johnston, Z. Lan, S. Law, E. MacLean, A. Trajman, D. Menzies, A. Benedetti, F. A. Khan, Diagnostic accuracy of serological tests for covid-19: systematic review and meta-analysis, *BMJ* (2020), <https://doi.org/10.1136/bmj.m2516>.
- [30] K.M. Koczula, A. Gallotta, Lateral flow assays, *Essays Biochem.* (2016), <https://doi.org/10.1042/EBC20150012>.
- [31] E. Stern, R. Wagner, F.J. Sigworth, R. Breaker, T.M. Fahmy, M.A. Reed, Importance of the debye screening length on nanowire field effect transistor sensors, *Nano Lett.* (2007), <https://doi.org/10.1021/nl071792z>.
- [32] I.I. Suni, Impedance methods for electrochemical sensors using nanomaterials, *TrAC Trends Anal. Chem.* (Reference Ed.) (2008), <https://doi.org/10.1016/j.trac.2008.03.012>.
- [33] E. Bakker, Y. Qin, Electrochemical sensors, *Anal. Chem.* (2006), <https://doi.org/10.1021/ac060637m>.
- [34] R. van den Hurk, S. Evoy, A Review of Membrane-based Biosensors for Pathogen Detection, *Sensors (Switzerland)*, 2015, <https://doi.org/10.3390/s150614045>.
- [35] Z. Slouka, S. Senapati, H.C. Chang, Microfluidic systems with ion-selective membranes, *Annu. Rev. Anal. Chem.* (2014), <https://doi.org/10.1146/annurev-anchem-071213-020155>.
- [36] G. Sun, Z. Pan, S. Senapati, H.C. Chang, Concentration-gradient stabilization with segregated counter- and Co-ion paths: a quasistationary depletion front for robust molecular isolation or concentration, *Phys. Rev. Appl.* (2017), <https://doi.org/10.1103/PhysRevApplied.7.064024>.
- [37] Z. Ramshani, C. Zhang, K. Richards, L. Chen, G. Xu, B.L. Stiles, R. Hill, S. Senapati, D.B. Go, H.-C. Chang, Extracellular vesicle microRNA quantification from plasma using an integrated microfluidic device, *Commun. Biol.* 2 (2019), <https://doi.org/10.1038/s42003-019-0435-1>.
- [38] S.S. Shah, S. Senapati, F. Klacsmani, D.L. Miller, J.J. Johnson, H.C. Chang, M. S. Stack, Current Technologies and Recent Developments for Screening of HPV-Associated Cervical and Oropharyngeal Cancers, 2016, <https://doi.org/10.3390/cancers8090085>, *Cancers (Basel)*.
- [39] D. Taller, K. Richards, Z. Slouka, S. Senapati, R. Hill, D.B. Go, H.C. Chang, On-chip surface acoustic wave lysis and ion-exchange nanomembrane detection of exosomal RNA for pancreatic cancer study and diagnosis, *Lab Chip* (2015), <https://doi.org/10.1039/c5lc00036j>.
- [40] Z. Yin, Z. Ramshani, J.J. Waggoner, B.A. Pinsky, S. Senapati, H.C. Chang, A non-optical multiplexed PCR diagnostic platform for serotype-specific detection of dengue virus, *Sensor. Actuator. B Chem.* (2020), <https://doi.org/10.1016/j.snb.2020.127854>.
- [41] Z. Slouka, S. Senapati, Y. Yan, H.C. Chang, Charge inversion, water splitting, and vortex suppression due to DNA sorption on ion-selective membranes and their ion-current signatures, *Langmuir* (2013), <https://doi.org/10.1021/la4007179>.

- [42] L.E. Mead, D. Prater, M.C. Yoder, D.A. Ingram, Isolation and characterization of endothelial progenitor cells from human blood, in: Current Protocols in Stem Cell Biology, John Wiley & Sons, Inc, 2007, <https://doi.org/10.1002/9780470151808.sc02c01s6>.
- [43] X. Zhang, Y. Zou, C. An, K. Ying, X. Chen, P. Wang, A miniaturized immunosensor platform for automatic detection of carcinoembryonic antigen in EBC, *Sensor. Actuator. B Chem.* (2014), <https://doi.org/10.1016/j.snb.2014.08.011>.
- [44] C. Wittmann, R.D. Schmid, Development and application of an automated quasi-continuous immunoflow injection system to the analysis of pesticide residues in water and soil, *J. Agric. Food Chem.* (1994), <https://doi.org/10.1021/jf00040a039>.
- [45] J.J. Van Der Pol, M. Machnik, M. Biselli, T. Portela-Klein, C.D. De Gooijer, J. Tramper, C. Wandrey, On-line immuno analysis of monoclonal antibodies during a continuous culture of hybridoma cells, *Cytotechnology* (1997), <https://doi.org/10.1023/A:1007913128209>.
- [46] J. Jantra, K. Zór, M. Sanders, S. De Saeger, M. Hedström, B. Mattiasson, Development of an automated flow-based spectrophotometric immunoassay for continuous detection of zearalenone, *Biotechnol. Appl. Biochem.* (2020), <https://doi.org/10.1002/bab.1876>.
- [47] Q. Pan, S. Hong, X. Zhu, M. Zhao, L.P. Lee, On-line electrophoretic sample clean-up for sensitive and reproducible μCE immunoassay, *Lab Chip* (2012), <https://doi.org/10.1039/c2lc21111d>.
- [48] D. Kim, Y.S. Lin, C.L. Haynes, On-chip evaluation of shear stress effect on cytotoxicity of mesoporous silica nanoparticles, *Anal. Chem.* (2011), <https://doi.org/10.1021/ac202115a>.
- [49] S. Marczak, E. Smith, S. Senapati, H.C. Chang, Selectivity enhancements in gel-based DNA-nanoparticle assays by membrane-induced isotachophoresis: thermodynamics versus kinetics, *Electrophoresis* (2017), <https://doi.org/10.1002/elps.201700146>.